Marine Chemistry 208 (2019) 56–69

Contents lists available at ScienceDirect

Marine Chemistry

journal homepage: www.elsevier.com/locate/marchem

The residence times of trace elements determined in the surface Arctic Ocean during the 2015 US Arctic GEOTRACES expedition

David Kadko[a,*], Ana Aguilar-Islas[b], Channing Bolt[b], Clifton S. Buck[c], Jessica N. Fitzsimmons[d], Laramie T. Jensen[d], William M. Landing[e], Christopher M. Marsay[c], Robert Rember[b], Alan M. Shiller[f], Laura M. Whitmore[f], Robert F. Anderson[g]

[a] Florida International University, Applied Research Center, Miami, FL, USA
[b] College of Fisheries and Ocean Sciences, University of Alaska Fairbanks, Fairbanks, AK, USA
[c] Skidaway Institute of Oceanography, University of Georgia, Savannah, GA, USA
[d] Department of Oceanography, Texas A&M University, College Station, TX, USA
[e] Department of Earth, Ocean and Atmospheric Science, Florida State University, Tallahassee, FL, USA
[f] Department of Marine Science, University of Southern Mississippi, Stennis Space Center, MS, USA
[g] Lamont-Doherty Earth Observatory, Columbia University, NY, USA

ARTICLE INFO

Keywords:
Trace elements
Residence times
Arctic Ocean
GEOTRACES

ABSTRACT

Data collected during the US Arctic GEOTRACES expedition in 2015 are used to estimate the mean residence time of dissolved trace elements (Fe, Mn, Ni, Cd, Zn, Cu, Pb, V) in surface water with respect to atmospheric deposition. The calculations utilize mixed layer trace element (TE) inventories, aerosol solubility determinations, and estimates of the atmospheric trace element flux into the upper ocean. The trace element flux is estimated by the product of the ^{7}Be flux (determined by the ocean ^{7}Be inventory) and the TE/^{7}Be ratio of aerosols. This method has been established elsewhere and is tested here by comparing ^{7}Be-derived TE flux to the measured TE accumulation in recently deposited snow. Given the variability in snow and aerosol TE concentration observed over the expedition, and the limited timescale of the observations, agreement between the two methods is reasonable. While there are assumptions in these calculations, the distribution of residence times with respect to atmospheric input across the expedition track informs us of additional sources or sinks for each element. The residence time of dissolved Fe was ~ 20–40 y for most stations. However, several stations that display a longer, oceanographically inconsistent apparent Fe residence time of ~300–500 years are likely influenced by additional input from the Transpolar Drift (TPD), which has been shown to convey shelf water properties to the central Arctic. This was seen for Cu, Ni and Zn as well. The flux of Fe delivered by the TPD was ~ 10 nmol/m^2/d for these stations, an order of magnitude greater than the soluble atmospheric input. On the other hand, V and Pb show a decrease in the apparent residence times within TPD water, suggesting removal of these elements from the source region of the TPD. For Mn, there is no obvious trend in residence time among the stations; however the apparent residence time (400–1400 y) is significantly greater than the ~20 y calculated for atmospheric input elsewhere, signifying appreciable input from other sources. It has been suggested that about 90% of Mn input to the Arctic Ocean originates from Arctic rivers, shelf sediments, and coastal erosion. Results here suggest a flux from these sources of ~30 nmol/m^2/d which is significantly greater than the atmospheric input of Mn in the Arctic.

1. Introduction

The residence time of atmospherically-delivered dissolved trace metals in the upper ocean informs us of several aspects of their biogeochemical behavior, including dissolution and scavenging processes, biological utilization, and the seasonal relationship of surface concentrations to atmospheric input (e.g. Jickells, 1999; Croot et al., 2004; Hayes et al., 2015; Bridgestock et al., 2016). Despite the utility of the concept, there are relatively few estimates of trace element (TE) residence times in the surface ocean, and heretofore none in the Arctic Ocean. This derives mainly from the difficulty in assessing atmospheric deposition rates which are rare and susceptible to problems of temporal

* Corresponding author at: Florida International University, Applied Research Center, 10555 W. Flagler St., Suite 2100, Miami, FL 33174, USA.
E-mail address: dkadko@fiu.edu (D. Kadko).

https://doi.org/10.1016/j.marchem.2018.10.011
Received 6 August 2018; Received in revised form 15 October 2018; Accepted 30 October 2018
Available online 12 November 2018
0304-4203/

and spatial variability (Kadko et al., 2015). In the Arctic for example, atmospheric transport and deposition of aerosols is an important delivery mechanism of natural and contaminant trace elements (e.g. Davidson et al., 1981, 1985; Barrie, 1986; MacDonald and Gobeil, 2011; Shaw, 1995; Stohl, 2006; Hov et al., 2007; Law and Stohl, 2007; Frossard et al., 2011; Zhan and Gao, 2014) but determination of deposition rates to this region has been limited by harsh conditions and infrequent research opportunities. Investigation of the source, residence time, and fate of atmospherically deposited trace elements in the surface ocean is challenging in general, but particularly so for the Arctic which has been the subject of relatively few studies (e.g. Klunder et al., 2012; Rijkenberg et al., 2018). While aerosol chemical concentrations collected from shipboard or land-based aerosol samplers are becoming more common, such concentration data by themselves cannot yield the deposition rate of trace elements. To transform these concentrations into rates, a method of determining flux is required. One method utilizes the tracer ^{7}Be, whereby the ability to derive the ^{7}Be atmospheric flux from the ocean/ice ^{7}Be inventory provides a means to link aerosol chemical concentrations to flux (Kadko et al., 2015, 2016; Slagter et al., 2017; Marsay et al., 2018a). Here, we utilize the ^{7}Be inventory in the Arctic Ocean and the TE/^{7}Be ratio of aerosols to estimate the atmospheric deposition of TEs measured during the 2015 US Arctic GEOTRACES expedition. The residence times with respect to atmospheric input of TEs in the surface ocean are then calculated with knowledge of 1) the aerosol TE solubilities, and 2) the inventory of dissolved TEs in that reservoir. The breadth of measurements afforded by the GEOTRACES program allowed these data to be assembled.

2. Background – ^{7}Be

Be-7 is a cosmic-ray produced isotope (half-life = 53.3 d) that is deposited upon the ocean surface primarily by precipitation and subsequently homogenized within the surface mixed layer (e.g. Young and Silker, 1980; Aaboe et al., 1981; Young and Silker, 1980; Kadko and Olson, 1996; Kadko, 2000; Kadko and Prospero, 2011; Kadko and Johns, 2011; Cámara-Mor et al., 2011; Haskell et al., 2015). While most of the production of ^{7}Be occurs in the stratosphere, the long residence time of aerosols in the stratosphere relative to the short half-life of ^{7}Be dictates that the tropospheric production of ^{7}Be determines the flux to the earth's surface although intrusions or vertical mixing of stratospheric components into the troposphere can occur (Feely et al., 1989; Dibb et al., 1994). Therefore, the ^{7}Be flux and water column inventory vary as a function of rainfall, and over broad oceanic regions are relatively constant. This is manifested by the observation that water column inventories are inversely related to surface salinity (Young and Silker, 1980; Kadko and Olson, 1996; Kadko and Johns, 2011).

2.1. Be-7 input

In the absence of physical removal processes other than radioactive decay, the water column inventory of ^{7}Be represents an integration of the atmospheric input flux over approximately the previous mean-life (77 d) of the isotope. With the relatively short half life of ^{7}Be, it has been demonstrated that the input flux of ^{7}Be (atoms $min^{-1}\,m^{-2}$) should be balanced by the ^{7}Be inventory, or decay rate, integrated over the water column (dpm m^{-2}) (e.g. Aaboe et al., 1981; Kadko and Prospero, 2011; Kadko et al., 2015). In these studies, open ocean standing crops of ^{7}Be matched the flux determined by nearby precipitation collectors. For example, between April 2007 and November 2008, the average oceanic ^{7}Be flux determined from the ocean inventories at the US JGOFS Bermuda Atlantic Time-Series site (BATS) and Hydrostation S, 60 km apart in the Sargasso Sea, were nearly identical to each other (0.048 ± 0.010 dpm cm^{-2} d^{-1}), and within error, matched the flux determined at Bermuda by precipitation collection (weighted average 0.051 ± 0.049 dpm cm^{-2} d^{-1}). This value is quite similar to that reported earlier for precipitation collected at the same site in Bermuda (0.047 dpm cm^{-2} d^{-1}) by Turekian et al. (1983). Thus, this 1-dimensional approach (no lateral effects) to first order appears valid due to the relatively short half life of ^{7}Be and the constancy of ^{7}Be deposition over broad latitudinal bands.

The mean life of ^{7}Be makes it extremely relevant to seasonal timescales, and the ability to derive the atmospheric flux of ^{7}Be from its ocean inventory provides a key linkage between the atmospheric concentration of TEs and their deposition to the ocean.

2.2. Determination of TE flux by the ^{7}Be method

It has been demonstrated that estimates of the atmospheric flux of trace elements (F_{TE}) can be made by multiplying the atmospheric flux of ^{7}Be by the [TE/^{7}Be] ratio in bulk aerosols, such that

$$F_{TE} = F_{7Be} \bullet \left[\frac{C_{TE}}{C_{7Be}}\right]_{aerosols} \quad (1)$$

where [C_{TE}/C_{7Be}] is the ratio of a trace element to ^{7}Be measured on aerosols (Kadko et al., 2015; Kadko et al., 2016; Shelley et al., 2017). The ^{7}Be flux, F_{7Be}, is derived from the measured ocean ^{7}Be inventory multiplied by the ^{7}Be decay constant.

Formulated in another way, the ratio F_{7Be}/C_{7Be} can be considered an effective bulk deposition velocity, V_b, which combines precipitation plus dry deposition (Young and Silker, 1980; Kadko et al., 2016). Then:

$$F_{TE} = V_b \bullet C_{TE} \quad (1b)$$

This method was initially tested offshore of Bermuda, where flux estimates for trace elements made by the ^{7}Be ocean inventory method were comparable to fluxes measured in rain samples collected on the island of Bermuda (Kadko et al., 2015). The situation at Bermuda allowed such testing to be made, where ocean-based methods could be calibrated by a convenient land location. The results suggested that the ^{7}Be method would be useful for remote areas where permanent sampling stations do not exist, such as the Arctic (Kadko et al., 2016).

Note that in the Arctic, Eq. (1) can be applied to separate reservoirs, such as the ocean, snow, and ice. Thus, measurement of the ^{7}Be inventory in each reservoir would yield an estimate of the TE accumulation by atmospheric deposition to that reservoir. An assumption in all cases is that the $[C_{TE}/C_{7Be}]_{aerosol}$ be constant over the timescale of the TE residence time with respect to atmospheric deposition. A comparison of historical ^{7}Be and trace metal data from Alert, Canada over a two- year period, 1990–1992, (Dibb et al., 1994; Dr. S. Sharma, personal communication; Kadko et al., 2016) with data from this study indicate that this is in general a good approximation. A summary of this data is presented in supplemental Table 1.

The organization of the paper is as follows. First, the total ^{7}Be inventory and its distribution between component compartments (ice + snow + melt pond, water column) will be presented and discussed. As ^{7}Be is a tracer of atmospheric input, this informs us about the disposition of TEs deposited by aerosols across the study transect and the extent to which ice intercepts the atmospherically deposited TEs. Next, the ^{7}Be inventories in freshly fallen snow are used to establish the "instantaneous" ^{7}Be flux at the time of the expedition. Multiplying this flux by the aerosol [TE/^{7}Be] ratio (Eq. (1), applied to the snow ^{7}Be inventory) provides an estimate of the TE accumulation during the onset of snowfall during this study. This is compared to the accumulation of TEs actually measured in the snow as a further test of the ^{7}Be method, analogous to the above-described rainfall tests made in Bermuda. Finally, the mean upper ocean residence times of dissolved trace metals (Fe, Mn, Ni, Cd, Zn, Cu, Pb, V) with respect to atmospheric deposition are calculated from their integrated water column inventories, the TE flux determined from Eq. (1) using the upper ocean ^{7}Be inventory, and the measured aerosol TE solubilities. The distribution of residence times across the expedition track informs us of additional sources or sinks for each element.

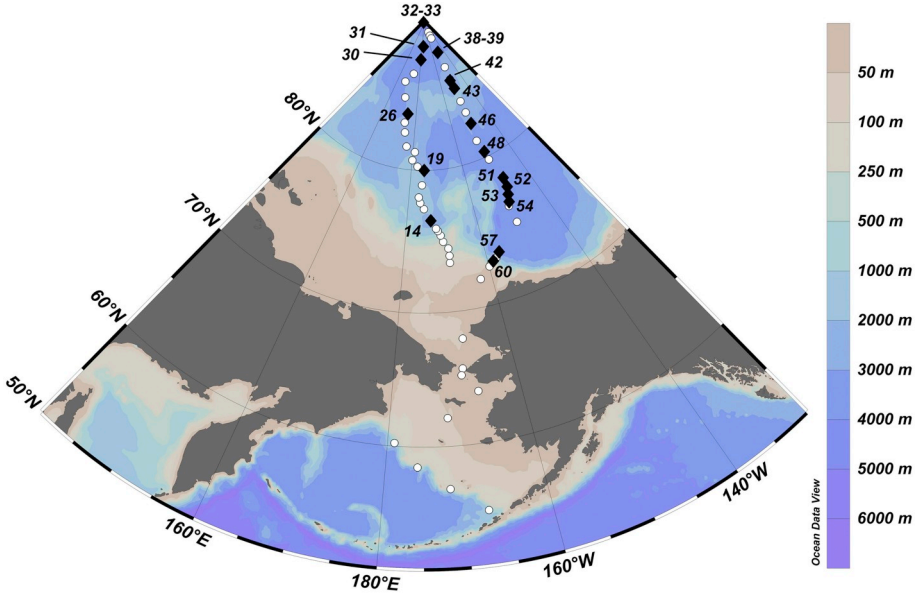

Fig. 1. The cruise track of US GEOTRACES Western Arctic research cruise (GN01) superimposed over bathymetry. Stations listed in Table 1 are indicated.

3. Methods

The US GEOTRACES Western Arctic research cruise (GN01) was carried out on USCGC *Healy* (cruise HLY1502) during late summer 2015, departing Dutch Harbor, Alaska, on August 9, 2015 and returning to Dutch Harbor on October 12, 2015. The cruise track, shown in Fig. 1, consisted of a northward transect through the Bering Strait and across the Makarov Basin to the North Pole, returning southward across the Canada Basin. Stations discussed in this paper (Table 1) are from water depths ≥1000 m as scavenging of ^{7}Be likely occurs in shallower, near shore environments (Olsen et al., 1986; Kadko and Swart, 2004).

3.1. ^{7}Be analysis

3.1.1. Seawater

Be-7 was analyzed by procedures described in detail elsewhere (Kadko et al., 2016). Briefly, a submersible pump was lowered from the ship to selected depths, delivering 400–700 l of seawater via a 1.5 in. hose into large plastic barrels on deck. From these barrels, the seawater was then pumped through iron-impregnated acrylic fibers at ~10 l/min (Lal et al., 1988; Krishnaswami et al., 1972; Lee et al., 1991). At times it was necessary to place submersible heaters in the barrels to prevent freezing. From occupations on the ice, water was pumped through hydroholes via a centrifugal pump directly through the Fe-fibers (Kadko, 2000). The pumping system was kept in a heated tent to prevent freezing. For both procedures, a portable CTD was attached to the end of the hose to record temperature and salinity. The efficiency of the fiber for Be extraction from seawater was previously determined to be 82–76% for sample volumes in the range 400–700 L, respectively. Back on shore, the fibers were dried and then ashed. To maximize ^{7}Be collection, generally two fibers, each filtering approximately 600 l of seawater were collected from each depth, combined, and placed in a Marinelli beaker, which in turn was placed over a low background germanium gamma detector. For some shallow samples where ^{7}Be activities were expected to be high, a single fiber batch was used and after drying and ashing was pressed into a pellet (5.8 cm diameter) and

Table 1
Station description.

Station	Date	Lat (deg N)	Long (deg E)	Depth (m)	ML[a] depth (m)	Σ depth (m)[b]
14	8/20/15	76.511	−173.034	2255	9.5	56
19	8/23/15	79.997	−174.962	2099	10	52
26	8/27/15	83.755	174.915	2938	18	52
30	9/01/15	87.520	−179.809	3943	19	46
31*	9/04/15	88.407	−176.761	3081	20	20
32–33*	9/05/15	89.987	−89.25	4236	14	23
38–39**	9/11/15	87.815	−149.734	2546	16	45
42*	9/14/15	85.731	−150.560	2961	nd	na
43**	9/15/15	85.135	−150.063	2204	32	41
46**	9/19/15	82.491	−149.872	3026	25	47
48	9/22/15	80.369	−149.855	3859	22	49
51	9/26/15	78.180	−147.831	3837	23	40
52	9/27/15	77.503	−148.009	3829	22	47
53	9/28/15	76.998	−148.803	3825	15	40
54	9/28/15	76.505	−149.515	3825	22	40
57	10/02/15	73.506	−156.808	3465	13	46
60	10/05/15	73.008	−158.729	994	13	36

* Indicates ice station.
** Indicates combined ship and ice stations.
[a] Mixed layer depth based on density.
[b] Depth of TE integration based on depth of ^{7}Be extinction (see Section 4.4).

Table 2
Snow, Ice and Melt Pond ^{7}Be Inventories[a].

Station	Sample date	Snow (dpm/m^2)[b]	Ice (dpm/m^2)[c]	Melt pond (dpm/m^2)[d]
31	9/4/2015	470 ± 20	2460 ± 305	na[e]
33	9/7/2015	425 ± 29	2055 ± 690	11,170 ± 760
39	9/11/2015	780 ± 51	1560 ± 300	4140 ± 810
42	9/14/2015	515 ± 16	1400 ± 210	3570 ± 500
43	9/16/2015	810 ± 34	3650 ± 450	2330 ± 345
46	9/19/2015	320 ± 15	1240 ± 450	3290 ± 210
	Average:	550 ± 170	2060 ± 820	3330 ± 3190

[a] Not corrected for the respective fractional areas.
[b] Measured ^{7}Be in a square meter of snow.
[c] Based on the sum of 3 cores (0.0064 m^2 each).
[d] Assumes melt pond depth is 1 m (Section 3.1).
[e] Not analyzed.

placed on a low background germanium gamma detector. Beryllium-7 decay produces a readily identifiable gamma peak at 478 keV. The detector was calibrated for each geometry by adding a commercially prepared mixed solution of known gamma activities to an ashed fiber(s) and counting the activities to derive a calibration curve. The uncertainty of the extraction efficiency (4%) and the detector efficiency (2%) was in all cases smaller than the statistical counting error and the uncertainty in the blank.

3.1.2. Melt pond water, ice, and snow samples

Melt pond samples consisted of 30–40 l of water from ponds which were frozen over at the time of sampling. The surface was broken through to collect water. Details of the sampling technique are given in Marsay et al. (2018b). Melt pond depths were not measured and are assumed to be less than the thickness of the sea ice (~1.5 m) but are > 30 cm which was the chosen sampling depth. A depth of 1 m is chosen for integrating the ^{7}Be content of the ponds (Table 2). This leads to uncertainty of ~50% in the integrated ^{7}Be value. As the melt pond contribution to the total ^{7}Be inventory ranges station-to-station from 0 to 35% (Fig. 2), this contributes approximately a 0–20% uncertainty to the total ^{7}Be inventory calculation. If the melt pound depth was only 0.5 m (Fetterer and Untersteiner, 1998; Skyllingstad and Paulson, 2007), then the total inventory would be overestimated by ≤20%. As described in Marsay et al. (2018b), variability in the ^{7}Be (and TE) content between the melt ponds arose predominantly from the different contributing fractions to each pond (i.e. snowmelt, ice melt, seawater).

Ice core samples were taken from the ice surface to the underlying seawater, producing a core 9 cm in diameter and generally ~1.5 m in depth. Three cores were combined (total area 0.019 m^2) for a single sample for ^{7}Be analysis to derive an integrated ^{7}Be inventory. When snow was present, it was removed from the surface of the ice prior to ice coring. Snow samples (from an area of 1m^2) were taken from the top of the ice and were 9–15 cm deep. The snow and ice samples were melted in pre-cleaned plastic buckets and received 5 ml of concentrated HCl, 5 mL of $FeCl_3$ in solution, and 0.5 ml of a stable Be tracer. After 12 h of equilibration, a concentrated NaOH solution was slowly added to co-precipitate the ^{7}Be with $Fe(OH)_3$ (Kadko, 2000; Eicken et al., 2002). The precipitate was returned to the lab where it was dried, placed in Petri dishes, and counted by gamma spectroscopy calibrated for this geometry. The precipitate was redissolved in dilute HCl and analyzed for stable Be by ICP-OES to calculate recovery yields.

3.1.3. Aerosol samples

As described in Marsay et al. (2018a), aerosol samples were collected using a Tisch Environmental TE-5170 V-BL high volume aerosol sampler, modified to collect 12 replicate aerosol samples on 47 mm open-face filter holders loaded with acid-washed Whatman-41 ashless filters for trace element analysis. The sampler was installed above the bridge of the ship to best sample clean air while avoiding sea spray.

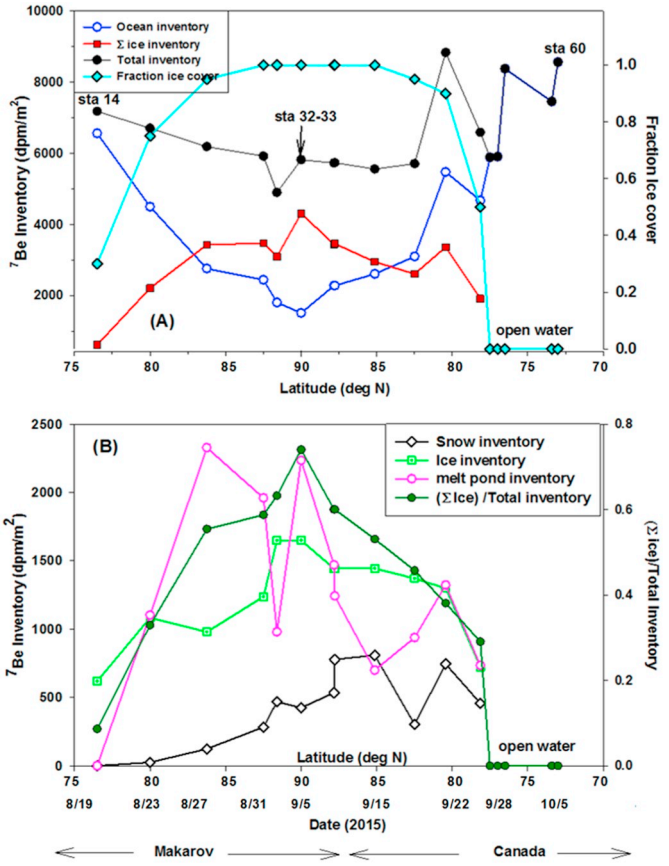

Fig. 2. A) The ocean (blue), [ice + snow + melt pond] (red) and total (black) ^{7}Be inventories for stations 14–60 across the US GEOTRACES transect. Note that as the fractional ice cover increases (cyan), the [ice + snow + melt pond] inventory increases while the ocean inventory decreases. B) The individual ice, snow, and melt pond inventories, and the fraction of ^{7}Be in the Σice cover relative to the total inventory. The ice inventories are based on the average ice concentration of all stations where ice was collected and the fractional ice-cover at each station. The derivation of snow inventories is described in Section 4.2. (For interpretation of the references to colour in this figure legend, the reader is referred to the web version of this article.)

Aerosol collection was limited to times when the relative wind direction precluded exhaust contamination from the ship's smokestack. For ^{7}Be, the Whatman-41 aerosol filters were stacked three-high in a plastic Petri dish and counted by gamma spectroscopy. This configuration was calibrated with a commercially prepared mixed solution of known gamma activities.

3.2. Trace element analyses

3.2.1. Seawater samples

Seawater was collected following established GEOTRACES sample collection protocols (Cutter and Bruland, 2012) using a trace metal-clean CTD on an epoxy-coated aluminum rosette mounted with 24 GO-Flo bottles (12*L*) on a Vectran conducting cable. Samples were filtered under ~0.5 atm pressure of filtered air in a sampling van through 0.2 μm Acropak-200 polyethersulfone capsule filters (Pall) into pre-cleaned low density polyethylene bottles (Nalgene) following three 10% volume rinses. Samples were acidified to pH 2 with ultrapure hydrochloric acid (Optima, to 0.012 M) and stored at least three months before analysis.

Samples were analyzed for their Fe, Mn, Zn, Cu, Cd, Ni, and Pb concentrations at Texas A&M University using isotope dilution for the multi-isotopic elements and matrix-matched standard curves for the

monoisotopic elements. Metals were extracted from seawater onto Nobias PA1 resin and pre-concentrated 25× using a SeaFAST-pico system (ESI, Omaha, NE) following a modified, offline version of the method of Lagerström et al. (2013). Elemental analysis was completed in low and medium resolution on a Thermo Element XR high-resolution inductively coupled-plasma mass spectrometer housed at the R. Ken Williams Radiogenic Isotope Facility. The accuracy of this method was validated by quantification of these dissolved metals in the SAFe D1 and D2 reference samples (supplemental Table 2).

Samples were analyzed for V at the University of Southern Mississippi whereby 14 ml of sample was spiked with isotopically-enriched ^{50}V, followed by extraction/pre-concentration using a SeaFAST system (Elemental Scientific, Inc.) operated in offline mode. A 10-ml sample loop was employed and the elution volume was 750 µl. A similar online SeaFAST extraction procedure is described by Hathorne et al. (2012) for rare earth elements. The extracted samples were subsequently analyzed using a Thermo-Fisher high resolution ICP-MS with an Apex-FAST high efficiency sample introduction system with Spiro desolvator (Elemental Scientific, Inc.). Besides measurement of ^{50}V and ^{51}V for isotope dilution measurement, ^{47}Ti and ^{52}Cr were monitored to correct for any ^{50}Ti or ^{50}Cr isobaric interference on ^{50}V; the correction was generally < 1%. Calibration was checked by analysis of a large-volume composite North Atlantic surface seawater sample. The reproducibility error of this method was estimated by comparing samples collected at the same depths on different casts at the same station. For 32 pairs of these replicate samples, the average absolute deviation was 0.8 nmol/kg or typically 2%. Repeated runs of US GEOTRACES intercalibration samples and in-house reference solutions suggest a precision of ± 1.5%; the limit of detection for vanadium was ~0.5 nmol/kg.

3.2.2. Snow samples

All sampling on the ice floes for TE measurements was conducted 30–50 m upwind of the ship to avoid ship exhaust. Skidoos were not used so as to avoid potential contamination of the ice environment. In addition, white 'clean room' suits were worn while sampling for snow and ice. Snow for TE analysis were collected with an acid cleaned polyethylene shovel used to transfer the snow column into an acid clean LDPE drum liner (18 mil; CDF Corporation), which was held inside a plastic bucket. Immediately after collection, the top of the drum insert was sealed over a plastic rod using plastic clamps. The sealed sample was transported to the ship, and the snow was allowed to melt at room temperature (~ 8–10 h). Upon melting, the sample was homogenized by gentle shaking, and a subsample was transferred to an acid cleaned 2 l HDPE bottle under HEPA filtered air. The subsample was filtered through a 47 mm diameter Supor polyethersulfone 0.2 µm filter disc held in a Teflon filter holder (Savillex). The filtrate was collected in LDPE bottles and acidified to pH < 1.7 with HCl (Optima grade). Filters containing particles were allowed to dry under HEPA filtered air and stored in LDPE bags. Analysis of TEs in snow samples was carried out at the University of Alaska Fairbanks on a Thermo-Scientific Element 2 HR-ICP-MS. Dissolved trace elements were quantified by isotope dilution using the SeaFAST system for on-line pre-concentration (Lagerström et al., 2013). Particulate trace elements were quantified with the use of a standard curve after complete digestion (Morton mix in Ohnemus et al., 2014).

3.2.3. Aerosol samples

As described in Marsay et al. (2018a), the aerosol filters were subjected to a three-stage strong acid digestion followed by determinations of total aerosol trace elements by a high-resolution inductively coupled mass spectrometer (HR-ICPMS; Thermo-Element 2) at the National High Magnetic Field Laboratory at Florida State University. The soluble aerosol fraction was measured using a variation of the flow-through extraction technique described in Buck et al. (2006). The aerosol-laden filter was placed in a Teflon filter holder over a 0.2 µm polycarbonate backing filter. While under vacuum, 100 ml of ultrapure deionized

Table 3
Water column ^{7}Be.

Station	Depth (m)	Collection Date	^{7}Be (dpm/m^3)	±
14	8	08/21/15	408.6	21.5
	14	08/21/15	110.5	18.1
	30	08/21/15	20.8	5.7
	56	08/21/15	14.6	9.7
19	7	08/23/15	277.2	15.9
	16	08/23/15	72.7	12.3
	30	08/23/15	24.8	9.5
	48	08/23/15	9.5	5.2
26	8.3	08/27/15	108.0	13.2
	26.4	08/27/15	26.1	7.3
	36.2	08/27/15	8.3	6.2
	46.8	08/27/15	8.0	5.3
30	9.6	09/01/15	90.3	11.4
	26.9	09/01/15	20.4	11.7
	35.9	09/01/15	20.5	6.3
	46	09/01/15	4.5	9.3
31 (ice sta)	0.5	09/03/15	92.2	7.3
	1.5	09/03/15	110.0	9.2
	5	09/03/15	105.5	8.2
	20	09/03/15	3.0	6.6
32	8.7	09/05/15	70.2	9.5
	21.4–22.9	09/05/15	bd	
	32.9	09/05/15	bd	
33 (ice sta)	0.5	09/07/15	110.2	20.6
	1.5	09/07/15	102.9	9.0
	5	09/07/15	97.9	8.8
38	10.1	09/10/15	85.8	9.7
	24	09/10/15	64.4	5.8
	29.7	09/10/15	21.9	6.5
	41.9	09/10/15	bd	
39 (ice sta)	0.5	09/11/15	75.6	14.5
	1.5	09/11/15	66.1	12.2
	5	09/11/15	82.8	11.7
42 (ice sta)	0.5	09/14/15	73.0	7.5
	1.5	09/14/15	64.2	7.7
43	20.4	09/15/15	75.2	18.8
	35	09/15/15	20.6	6.7
	40.8	09/15/15	bd	
	45.8	09/15/15	bd	
43 (ice sta)	0.5	09/16/15	68.9	11.7
	1.5	09/16/15	65.1	15.4
	5	09/16/15	57.1	8.9
46	21.1	09/18/15	96.2	17.1
	28.9	09/18/15	16.4	9.7
	40.7	09/18/15	26.4	10.0
	46.9	09/18/15	16.3	10.3
46 (ice sta)	0.5	09/19/15	120.1	12.6
	1.5	09/19/15	142.2	16.1
	5	09/19/15	103.1	12.6
48	16.5	09/22/15	181.4	19.0
	31.6	09/22/15	53.6	11.7
	42	09/22/15	9.6	9.7
	48.8	09/22/15	bd	
51	6.7	09/26/15	177.0	14.9
	27.9	09/26/15	20.2	12.0
52	12.5	09/27/15	221.3	19.8
	27.5	09/27/15	39.1	16.6
	38.2	09/27/15	9.5	12.0
	46.8	09/27/15	bd	
53	5.5	09/28/15	278.6	11.7
	25	09/28/15	26.7	16.9
54	6	09/28/15	353.7	47.2
	24	09/28/15	7.5	6.9
57	12.5	10/02/15	351.0	24.6
	24	10/02/15	52.7	18.0
	34	10/02/15	26.8	11.4
	46	10/02/15	19.3	11.2
60	6.4	10/05/15	378.4	33.6
	25.4	10/05/15	113.1	13.9

bd. Below detection.

Table 4
Snow trace element concentrations.

Sta	Mn (nM)			Fe (nM)			Ni (nM)			Cu (nM)		
	Dissolved	Part	Total	Dissolved	Part	Total	Dissolved	Part	total	Dissolved	Part	total
31	1.33	3	4.33	8.3	390	398.3	0.030	0.49	0.52	0.12	0.27	0.390
33	3.36	20.5	23.86	5.8	2580	2585.8	0.038	2.78	2.82	0.18	0.9	1.075
39	0.50	0.23	0.73	1.3	15.1	16.4	0.064	0.16	0.22	0.17	0.11	0.280
42	4.37	0.43	4.80	2.3	34.2	36.5	0.485	0.45	0.94	0.60	0.3	0.895
43	0.45	0.15	0.60	2.5	7.7	10.2	0.045	0.01	0.06	0.56	0.03	0.590
46	0.30	0.33	0.63	1.2	25.4	26.6	0.030	0.19	0.22	0.19	0.13	0.315

	Zn (nM)			Cd (nM)			Pb (nM)			V (nM)		
	Dissolved	Part	Total	Dissolved	Part	total	Dissolved	Part	Total	Dissolved	Part	Total
31	17.82	1.53	19.35	0.0045	0.006	0.010	na	2.3	2.30	na	1.46	> 1.46
33	12.45	8.95	21.40	0.0025	0.019	0.022	0.00645	15.8	15.81	0.2	8.88	9.08
39	9.61	0.03	9.64	0.0020	0.005	0.007	0.032	0.08	0.11	0.3	0.32	0.62
42	12.33	0.92	13.25	0.0070	0.01	0.017	0.11	0.2	0.31	0.7	0.39	1.10
43	8.13	0.12	8.25	0.0022	0.007	0.009	0.057	0.31	0.37	0.1	0.06	0.17
46	7.35	0.09	7.44	0.0026	0.012	0.015	0.037	0.14	0.18	0.1	0.37	0.47

water (> 18 MΩ·cm) was poured over the filter and the leachate solution collected in a 100 ml LDPE bottle. Following acidification with Teflon-distilled hydrochloric acid, the samples were analyzed for trace element concentration by a quadrupole inductively coupled mass spectrometer (Perkin Elmer Nexion 300D) coupled with a SeaFAST S2 sample introduction and preconcentration system (Elemental Scientific) at the Skidaway Institute of Oceanography.

3.3. Fraction ice and melt pond coverage

Hourly estimates of fractional ice coverage were provided by the USCGC Healy. This was augmented by post-cruise analysis of photographs taken hourly by the automatic, forward looking aloft con camera (Dimento et al., n.d). The sea ice coverage trend along the cruise track is shown in Fig. 2. For the period August 23–September 10, melt pond coverage estimates were made quasi-daily at sea and from post cruise evaluation of the aforementioned aloft con camera. These values were in the range 0.2–0.5, which is consistent with observations made elsewhere (Tschudi et al., 2008; Eicken et al., 2002). After September 10, deepening snow precluded estimating melt pond coverage and a value of 0.3 was used in subsequent calculations (Fetterer and Untersteiner, 1998; Tschudi et al., 2008).

4. Results and discussion

The snow, ice and melt pond ^{7}Be inventory data are presented in Table 2, and the water column ^{7}Be data in Table 3. Dissolved and particulate trace element concentrations in snow are shown in Table 4. Aerosol activities of ^{7}Be and trace element concentrations have been presented in Marsay et al. (2018a) and are summarized in Table 5, and elemental aerosol solubilities are shown in Table 6.

Table 6
Elemental aerosol solubilities

	Mn	Fe	Ni	Cu	Zn	Cd	Pb	V
Mean	34%	1%	21%	32%	51%	52%	21%	15%
SD	26%	2%	26%	28%	39%	34%	21%	24%

4.1. Total ^{7}Be inventories

Fig. 2a shows the ocean, ΣIce = [ice + snow + melt pond], and total (ΣIce + ocean) inventories of ^{7}Be for stations 14–60 across the 2015 US GEOTRACES transect. The individual ice, snow, and melt pond ^{7}Be inventories are shown in Fig. 2b. The ice inventories are based on the average of all the ice concentrations and the fractional ice cover for the individual station. The snow inventories are based on individual station measurements or on estimates for the stations where snow was not collected (see 4.2 below).

As might be expected for a relatively constant ^{7}Be flux across the region, as the fractional ice cover increases the ΣIce inventory increases, and the ocean inventory decreases. This has been observed in other works (Cámara-Mor et al., 2011; Kadko et al., 2016). Since ^{7}Be is a tracer of atmospheric input, this suggests that atmospherically transported species should be similarly intercepted by the ice floe (Cámara-Mor et al., 2011). Where ice cover approaches 100%, a significant proportion of ^{7}Be is found in the ice cover (Σ Ice), which approaches 70% of the total at the N. Pole where the water column inventory is at a minimum (Fig. 2b). Snow-fall commenced on or about August 23, and thereafter snow became increasingly significant as an aerosol catchment as the fall season progressed.

The total ^{7}Be inventory across the transect ranged between 4600 and 8800 dpm/m^{2} (average 6400 dpm/m^{2}). By comparison, Kadko

Table 5
Mean aerosol concentrations.

	Mn	Fe	Ni	Cu	Zn	Cd	Pb	V
aerosol TE (nmol/m^{3})[a]	0.0015 ± 0.0021	0.077 ± 0.090	0.0014 ± 0.0009	0.0076 ± 0.0065	0.030 ± 0.025	0.0029 ± 0.0026	0.0019 ± 0.0017	0.00027 ± 0.00036
aerosol TE/^{7}Be (nmol/dpm)[a,b]	0.045 ± 0.062	2.28 ± 2.65	0.042 ± 0.027	0.224 ± 0.192	0.885 ± 0.727	0.086 ± 0.075	0.056 ± 0.050	0.008 ± 0.011

[a] Data from Marsay et al. (2018a). These are the average of 13 measurements taken between Aug 10 and Oct 7, 2015 during the US GEOTRACES cruise.
[b] Average ^{7}Be aerosol = 0.034 ± 0.008 dpm m^{-3}.

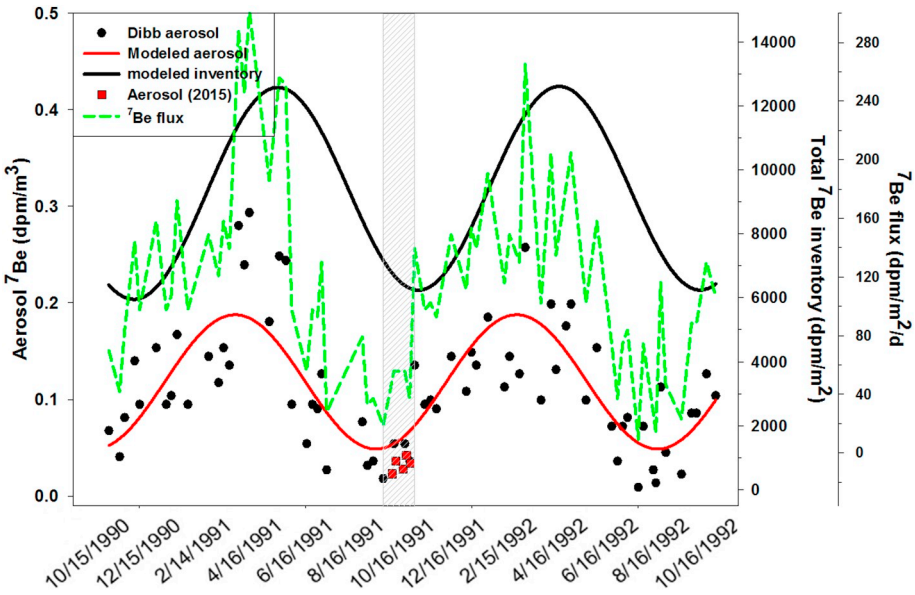

Fig. 3. Aerosol ^{7}Be concentrations in this study (red squares) compared to those measured in a two-year study at the Alert, Canada site by Dibb et al. (1994) (black circles). The shaded area delineates the time-of-year of the 2015 US GEOTRACES cruise. The sine fit to the Dibb et al. data is shown as the red line. The ^{7}Be inventory derived from the modified sine fit to the Dibb et al. aerosol time-series is shown as a black line (see text) and was tuned to match the average inventory we measured (6400 dpm/m^2) by using an effective bulk (wet plus dry) deposition velocity (V_b) of 1030 m/day. The ^{7}Be flux calculated from the aerosol activities and V_b is shown by the dashed green line. (For interpretation of the references to colour in this figure legend, the reader is referred to the web version of this article.)

et al. (2016) reported a range of 5500–13,000 dpm/m^2 (average 8400 dpm/m^2) for the eastern central Arctic and Cámara-Mor et al. (2011) reported a value of 7800 dpm/m^2 for a transect in the Eurasian Basin. The uncertainty in the total inventory arises from uncertainties in estimating fractional ice and melt pond coverage, as well as from the difficulty in assessing average ice, snow and melt pond inventories based on only limited samples, and the unknown heterogeneity of these values across a given ice floe.

The ^{7}Be flux method was first developed in waters off Bermuda where the seasonal variability of the aerosol ^{7}Be activity over Bermuda is only about a factor of 2–3 (Arimoto et al., 1999; Kadko et al., 2015) with the consequence that the cumulative ^{7}Be ocean inventory, from progressive input and decay of the input flux, does not vary by > 20% throughout the year (Kadko and Prospero, 2011; Kadko et al., 2015, 2016). Therefore, the ocean inventory measured at any one time is representative (to within 20%) of the instantaneous ^{7}Be flux. However, in the Arctic, the situation is more complicated, as the ^{7}Be aerosol activity exhibits significant seasonal variability of an order of magnitude arising from migration of the polar front and to a lesser extent variable stratospheric input (Dibb et al., 1994; Fig. 3). Significant seasonal variability is also observed for many other chemical species in the Arctic (e.g. Barrie, 1986; Douglas and Sturm, 2004). To estimate the effect of the seasonal variability in the ^{7}Be aerosol activity on the Arctic Ocean ^{7}Be inventory, a sine fit to the Dibb et al. (1994) aerosol data was constructed and the expected ^{7}Be water/ice/snow inventory from the daily input of aerosol ^{7}Be and decay of the ^{7}Be that had been deposited on previous days was calculated, summed over "n" days (Kadko et al., 2016):

$$[\text{Inventory 7Be}] = \sum_{i=1}^{n} [\,Cp_{7Be,i} + Cp_{7Bei-1}\cdot\exp.(-\lambda\Delta T)]\Delta T\cdot Vb \quad (2)$$

where [Inventory ^{7}Be] is the modeled ^{7}Be inventory of the water/ice/snow system (dpm/m^2), $Cp_{7Be,\,i}$ = ^{7}Be aerosol concentration on day "i" (dpm/m$^3_{air}$), $Cp_{7Be,\,i-1}\cdot e(-\lambda\Delta T)$ is the ^{7}Be aerosol concentration on the previous day corrected for radioactive decay (dpm/m$^3_{air}$), and ΔT is one day in time. This is equivalent to the cumulative daily ^{7}Be inventory decay and flux input such that the inventory on any day "n" is

$$[\text{Inventory}^{7}\text{Be}]_n = [\text{Inventory}^{7}\text{Be}]_{n-1}\cdot(\exp(-\lambda\Delta T) + [Cp_{7Be,n}]\,\Delta T\cdot V_b \quad (2b)$$

The term V_b is the bulk aerosol deposition velocity (Young and Silker, 1980; Marsay et al., 2018a) defined by:

$$V_b = \frac{\text{Flux (dpm m}^{-2}\text{d}^{-1})}{\text{Aerosol Concentration (dpm m}^{-3})} \quad (3)$$

The results are shown in Fig. 3, where the modeled ^{7}Be inventory was tuned to match the average measured total ^{7}Be inventory (~6400 dpm/m^2) during the GEOTRACES expedition by using an effective deposition velocity of 1030 m/day (Eq. (2)).

Given that the observed total (ΣIce + ocean) inventory across the transect ranged between 4600 and 8800 dpm/m^2, the range of deposition velocity is 740–1420 m/day, comparable to the value of 1350 m/d presented in Kadko et al. (2016) for the central Arctic and the depositional velocity of 1900 ± 950 m/day derived by Davidson et al. (1985) for aerosol deposition on the Greenland ice sheet. By comparison, treating the time-series ^{7}Be aerosol data of the Bermuda study (Kadko et al., 2015) with Eq. (2), requires a deposition velocity of ~2600 m/d to match the measured ^{7}Be ocean inventory. This is consistent with the greater precipitation rate over the N. Atlantic compared to the Arctic Ocean.

Application of this same effective deposition velocity throughout the year yields a ^{7}Be flux that is dependent only on the aerosol concentration. Using the Dibb aerosol concentrations and an effective V_b of 1030 m/day, the ^{7}Be flux reaches a maximum of 300 dpm/m^2/d in mid-March and a minimum in late August of ~20 dpm/m^2/d (Fig. 3). The fluxes predicted by the aerosol concentrations measured during the GEOTRACES cruise (mid-August to late September) using the derived deposition velocity are 24–45 dpm/m^2/d. The model ^{7}Be inventory varies from a maximum of ~12,600 dpm/m^2 in late March to a minimum of ~6200 dpm/m^2 in early October (Fig. 3).

4.2. *^{7}Be inventory in snow*

As discussed in Marsay et al. (2018a), the GEOTRACES cruise overlapped the onset of snowfall which allowed several samples of recently fallen snow to be collected and from those the instantaneous values of ^{7}Be flux estimated using

$$F_{7Be} = \lambda A_s/(1 - \exp(-T\lambda)) \quad (4)$$

where: λ = ^{7}Be decay constant (0.013 d^{-1}), A_s is the snow inventory of ^{7}Be per m^2, and T is the time between onset of snowfall and collection date. Initial observations of snowfall were recorded on August 23, and this is assumed to be representative of the snowfall initiation date for stations subsequently sampled for snow. It is unlikely that all stations had identical snow-fall histories, and likely there was heterogeneity of

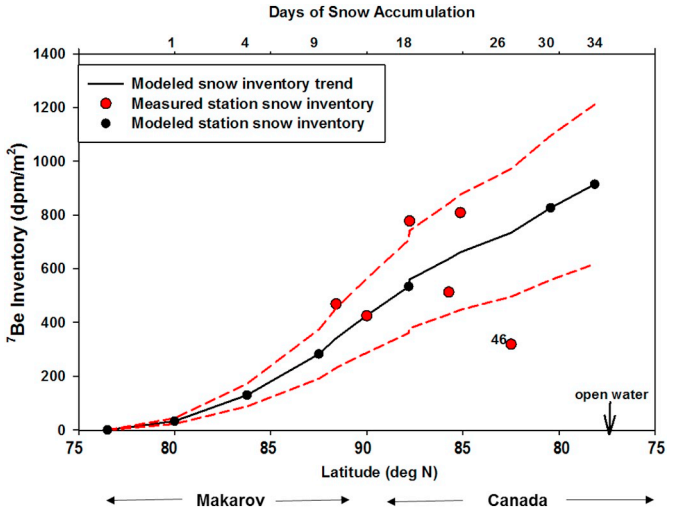

Fig. 4. Inventories of ^{7}Be measured in snow at occupied ice stations (red dots). The black line shows the trend predicted from Eq. (5), with ^{7}Be flux = 33 ± 11 dpm/m^2/d, and the black dots are estimates for stations where snow was not collected. The dashed red lines encompass the standard deviation of the flux. Station 46 is indicated. The presumed days of snow accumulation are shown. (For interpretation of the references to colour in this figure legend, the reader is referred to the web version of this article.)

accumulation within any one site. Nonetheless, application of Eq. (4) to the inventories of each site (Table 2) yields a calculated flux for each station that falls within a relatively narrow range defined by an average of 33 ± 11 dpm/m^2/d. This falls squarely within the range (24–45 dpm/m^2/d, Fig. 3) modeled by the total system ^{7}Be inventory and the Dibb et al. (1994) time-series aerosol concentration discussed above in Section 4.1, for the timeframe of the GEOTRACES cruise.

The snow-derived ^{7}Be flux (33 ± 11 dpm/m^2/d) can be combined with the average ^{7}Be aerosol activity (0.034 ± 0.008 dpm/m^3) to yield a bulk aerosol deposition velocity, V_b, as defined by Eq. (3). A value of ~980 m/d (range 535-1665 m/d) is obtained which is comparable to the value of 1030 m/d derived above using the total ^{7}Be inventories and the Dibb et al. (1994) time-series aerosol concentration in Section 4.1.

The average ^{7}Be flux determined by the ^{7}Be inventory in the newly-fallen snow represents an instantaneous flux, reflecting the most recent aerosol input. The steady state inventory that this flux would support is ~2600 ± 830 dpm/m^2, which is less than half that observed for the total water/ice system during the GEOTRACES transect (Fig. 2a). The aerosol activities measured at that time were quite low, but consistent with those reported in Kadko et al. (2016) and Dibb et al. (1994) for the same time of year (late summer) in the Arctic. However, in the Arctic, aerosol ^{7}Be activities early in the year (February–April) are up to an order of magnitude larger than those in the summer months (Fig. 3). Thus, the high ^{7}Be inventories observed in the ocean-ice system during GEOTRACES are to some extent a remnant of earlier deposition maintained during the isotope's 2.5 month mean-life (Eq. (2)) but would not be reflected in the recent snow.

The snow flux can be used to construct a trend of the ^{7}Be inventory in snow for the entire GEOTRACES transect, allowing estimates of the snow inventory when snow data are not available. The inventories would be expected to increase with time approaching a steady-state value after several half-lives of ^{7}Be according to:

$$A_s = F_{7Be}(1 - \exp(-T\lambda))/\lambda \quad (5)$$

which is a rearrangement of Eq. (4), where again, T is the time between the onset of snowfall and the collection date. Fig. 4 shows the inventories of ^{7}Be measured in snow at occupied ice stations and those estimated using Eq. (5) for stations where there were no ice occupations. With the exception of station 46, the ^{7}Be inventories of occupied

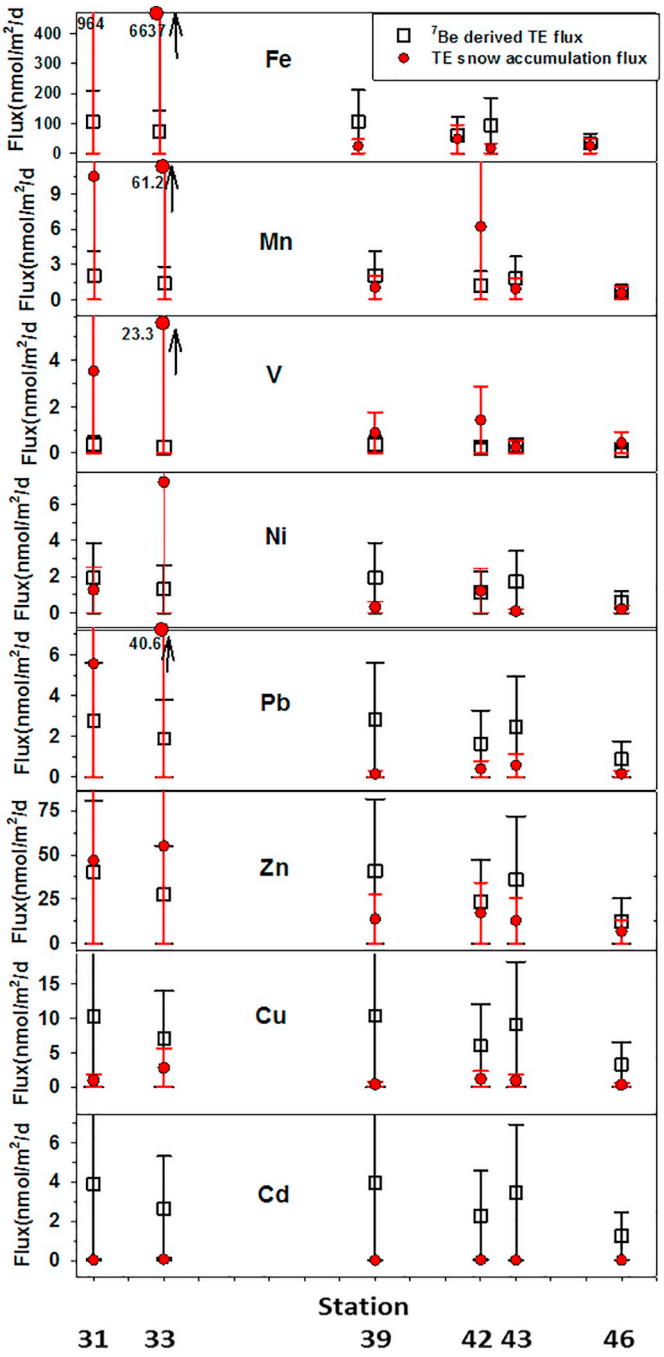

Fig. 5. Trace element fluxes determined by the ^{7}Be method (squares) and by integration of the trace element content of snow (red dots). (For interpretation of the references to colour in this figure legend, the reader is referred to the web version of this article.)

stations are comparable to the predicted trend. This plot was used to construct the snow inventory plot of Fig. 2b.

4.3. Trace element fluxes

The goal of this work is to derive the surface ocean residence time of atmospherically deposited TEs in the Arctic using the TE flux derived from the ^{7}Be inventory of the upper ocean and the [C_{TE}/C_{7Be}] ratio of aerosols falling into the ocean (Eq. (1)). This method was initially tested at Bermuda, where rain collectors were deployed at the Bermuda Institute of Ocean Science (BIOS) such that TE fluxes collected there could be compared to those calculated from the product of nearby ocean ^{7}Be

inventories and the [C_{TE}/C_{7Be}] aerosol ratio. In that study, fluxes of TEs determined by the rain collectors and by the ^{7}Be method agreed to within a factor of 2 (Kadko et al., 2015).

In the Arctic no such opportunity exists, but as described above, several samples of recently (< 1 month) fallen snow were collected, and an approximate date of snowfall onset is known. With this information instantaneous values of ^{7}Be and TE flux can be estimated and used to test the ^{7}Be method. Fig. 4 indicates that this worked well for ^{7}Be, suggesting an uncertainty of < 50% for that isotope. Marsay et al. (2018a) calculated the average bulk deposition velocity (V_b) from the average ^{7}Be flux (derived from the ^{7}Be inventory) of the snow samples collected from all sites and the average aerosol ^{7}Be activity of the cruise (Eq. (3)). The average TE flux was then derived from the product of the average V_b and the average aerosol [TE] across the GEOTRACES transect (Eq. (1b)). Average aerosol TE deposition fluxes based on this approach are presented in that work.

Here, we compare fluxes determined by the ^{7}Be inventory method applied to each individual snow sample with the TE inventories actually measured in the snow. The results are shown in Fig. 5. This will serve as a test which is analogous to the rain collection exercise reported at Bermuda (Kadko et al., 2015). The ^{7}Be – based estimates are calculated from the mean aerosol [TE/^{7}Be] ratio and the ^{7}Be flux (i.e. ^{7}Be inventory) of each snow sample (Eq. (4), see data in Table 2 and Fig. 2). The mean aerosol data shown in Table 5 display considerable variability between aerosol samples (Marsay et al., 2018a) which contributes appreciable uncertainty to this calculation. Results shown in Fig. 5 indicate the large error bars (black lines) associated with this variability. This ^{7}Be-derived estimate is compared to the observed TE flux which is based on the measured TE inventory in snow:

$$\text{Flux} = \text{TE concentration x } \rho \text{ x snow depth/days of snowfall} \quad (6)$$

where TE concentration is the trace element concentration (nM) of melted snow (Table 4), and ρ = ratio of the density of snow to that of water. Snow density was not determined during the GEOTRACES expedition. Warren et al. (1999) report monthly mean snow densities for the Arctic and determined that for August–September the density is 250 ± 100 kg/m^3. This contributes a factor of 2 uncertainty in this calculation indicated by the red error bars in Fig. 5.

There was geographic variability in this comparison, but patterns between stations and across elements did emerge. The first two snow stations had a large particle content. This was particularly so for station 33, as was also observed for the melt pond sampled at this station (Marsay et al., 2018b). The trace element fluxes determined from the snow TE inventory for this station were higher by far than those determined by the ^{7}Be method. Neglecting station 33, the average station fluxes by the two methods were comparable (within a factor of ~3) for Mn, Fe, Pb, Zn and Ni, while for V the average comparison was within a factor of ~5.

In contrast, the Cu and Cd flux predicted using ^{7}Be were factors of ~10 and 100, respectively, greater than those derived from the accumulation of these TEs in the snow. Interestingly, the Cu/Al and Cd/Al ratios of melt pond particles were, respectively, > 10 and > 100 times that of upper continental crust as were the average aerosol Cu/Al and Cd/Al ratios (Marsay et al., 2018a, 2018b). The lack of such a signal in the snow is therefore perplexing, but perhaps reflects short term variability in snow and aerosol concentrations while melt pond particles reflect longer term input. The ^{7}Be method relies on the ^{7}Be in the snow and the TE/^{7}Be ratio in aerosols. The snow inventory method integrates the TE content of the snow. There is uncertainty in this comparison because of the variability in both snow and aerosol TE concentration observed over the expedition, and the limited timescale of observation. Such variability is not surprising; Klunder et al. (2012) discuss the wide range of dissolved and particulate Fe in snow samples taken relatively close to each other. There has also been observation of seasonal and episodic (short-duration intrusions of aerosol-laden air) variability in aerosol samples collected from areas around the Arctic (Pacyna and Ottar, 1985; Sirois and Barrie, 1999). Davidson et al. (1985) reported highly variable particle and TE concentration in Greenland aerosols on a day-to-day basis. This complicates direct comparison of aerosol concentrations to snow-fall trace element fluxes. In addition, using aerosol concentrations averaged over the transect might not be representative of the material actually collected in any one snow sample. By contrast, applying the ^{7}Be method to the water column encompasses a much longer integration period (several months, not 2–3 weeks); the variable chemical composition of atmospheric input will be integrated towards average values such that daily variability will be of less significance (Section 4.4). Given the variability in snow and aerosol TE concentration observed over the expedition, and the limited timescale of the observations, agreement between the two methods is reasonable.

Size fractionated aerosol trace metal data were not available for this study, but discussion in Kadko et al., (2015) and the agreement here of the ^{7}Be method with the TE accumulation in snow suggest that size differences between TE and ^{7}Be -bearing particles do not contribute significant error to our approach. In our formulation, the constancy of the TE/^{7}Be ratio on aerosols, as discussed earlier, is of greater importance.

Finally, the situation in this Arctic study was unique because the GEOTRACES cruise overlapped the onset of snowfall such that the approximate period of TE accumulation could be determined. Otherwise snow accumulation rates, and thus TE accumulation rates in the Arctic are difficult to ascertain (e.g. Davidson et al., 1985). The ^{7}Be method offers an alternative, circumventing this problem as well as the difficulty of clean sampling of TEs in snow.

4.4. Trace element residence times for the upper ocean

Potential fluxes of trace metals to the surface Arctic Ocean include atmospheric deposition, riverine supply, advection from the Pacific or Atlantic oceans, and input from shelf sediments. Because ^{7}Be is an unambiguous tracer of atmospheric deposition, we can solve for the atmospheric flux of metals (Eq. (1)) to gain perspective of the importance of this flux relative to other potential input terms. We start by assuming atmospheric input is the dominant flux to the Arctic and calculate a residence time with respect to this atmospheric deposition. We then compare this "apparent residence time with respect to atmospheric input" with residence times determined in other remote areas of the ocean, known to be dominated by atmospheric inputs, to learn the extent to which Arctic Ocean metals are sourced by other fluxes.

The mean apparent residence time of dissolved trace metals with respect to atmospheric deposition, τ, is given by:

$$\tau = M/F_{TE(sol)} \quad (7)$$

where M is the inventory of the dissolved trace element in surface water derived from integrating the dissolved TE concentrations to the depth where ^{7}Be is extinguished (Table 1). This corresponds to the maximum annual mixed layer depth of ~50 m during the spring (Maykut and McPhee, 1995; Morison and Smith, 1981; Kadko, 2000) which in the Arctic is delineated by strong density stratification. The ^{7}Be, trace element, and density profiles are shown in Fig. S1. $F_{TE(sol)}$ is the soluble aerosol flux. Assuming that the most biogeochemically relevant fraction of atmospheric flux is that which is operationally defined as soluble, we adjust Eq. (1) to account for the elemental aerosol fractional solubility, α, so that F_{TE} becomes:

$$F_{TE(sol)} = F_{7Be} \bullet \left[\frac{C_{TE}}{C_{7Be}}\right] \bullet \alpha \quad (8)$$

The ^{7}Be flux (F_{7Be}) is derived from the measured ocean ^{7}Be inventory multiplied by the ^{7}Be decay constant and is listed in Table 7 for each station. Atmospheric input is assumed to be the only source for the dissolved trace elements, such that the resulting residence time is

Table 7
Residence times (τ, years).

Station	Flux ^{7}Be[a]	Flux Fe[b]	M ΣFe[c]	Fe τ[d]	Flux Mn[b]	M ΣMn[c]	Mn τ[d]	Flux Ni[b]	M ΣNi[c]	Ni τ[d]	Flux Cd[b]	M ΣCd[c]	Cd τ[d]
14	85	194	2.48×10^4	35	3.83	2.67×10^5	560	3.6	3.73×10^5	1360	7.2	19100	13.9
19	58.5	133	2.03×10^4	42	2.63	3.64×10^5	1115	2.5	4.26×10^5	2260	5.0	22550	23.9
26	36	82	1.26×10^4	42	1.62	2.46×10^5	1225	1.5	3.58×10^5	3095	3.1	17340	29.9
30	32	73	8.44×10^4	315	1.44	2.48×10^5	1390	1.3	3.61×10^5	3510	2.7	14960	29.1
31	17	40	7.3×10^4	500	0.78	0.86×10^5	885	0.7	1.70×10^5	3045	1.5	6100	21.7
32–33	20	45	8.2×10^4	500	0.89	1.23×10^5	1125	0.8	1.81×10^5	2850	1.7	6100	19.2
38–39	30	67	1.16×10^5	475	1.33	1.57×10^5	950	1.2	3.61×10^5	3800	2.5	12500	26.1
43	34	78	1.52×10^5	535	1.53	2.0×10^5	1055	1.4	3.48×10^5	3180	2.9	11400	20.8
46	40	91	1.21×10^4	36	1.80	2.46×10^5	1100	1.7	3.29×10^5	2555	3.4	14275	22.1
48	71	162	1.26×10^4	21	3.2	2.44×10^5	615	3.0	3.35×10^5	1465	6.0	15800	13.8
51	61	139	0.92×10^4	18	2.75	2.24×10^5	660	2.6	2.66×10^5	1355	5.2	11700	11.9
52	76.5	174	1.37×10^4	22	3.44	2.64×10^5	620	3.2	3.175×10^5	1290	6.5	14100	11.4
53	77	175	1.13×10^4	18	3.46	2.08×10^5	485	3.2	2.74×10^5	1110	6.5	11190	9.0
54	109	248	1.19×10^4	13	4.90	2.28×10^5	375	4.6	2.77×10^5	790	9.3	11230	6.4
57	97	221	1.375×10^4	17	4.37	2.46×10^5	455	4.1	3.01×10^5	965	8.2	12410	7.9
60	117	267	2.91×10^4	30	5.3	3.82×10^5	580	4.9	2.91×10^5	775	10.1	12200	6.4

	Flux Zn[b]	M ΣZn[c]	Zn τ[d]	Flux Cu[b]	M ΣCu[c]	Cu τ[d]	Flux Pb[b]	M ΣPb[c]	Pb τ[d]	Flux V[b]	M ΣV[c]	V τ[d]
14	75	6.85×10^4	4.9	19	2.25×10^5	101	4.8	250	0.69	0.68	1.18×10^6	32000
19	52	7.16×10^4	7.4	13	2.68×10^5	175	3.3	190	0.76	0.47	1.42×10^6	56000
26	32	7.52×10^4	12.7	8.1	2.08×10^5	221	2.0	145	0.94	0.29	1.07×10^6	73000
30	28	5.43×10^4	10.3	7.2	2.66×10^5	318	1.8	32.5	0.24	0.26	0.66×10^6	45000
31	15	7.6×10^4[e]	26.5[e]	3.9	1.63×10^5	357	1.0	56.5[e]	0.76[e]	0.14	0.27×10^6	37000
32–33	17	4.2×10^4	12.9	4.4	1.55×10^5	301	1.1	23	0.27	0.16	0.34×10^6	47000
38–39	26	3.97×10^4	8.1	6.6	2.82×10^5	364	1.7	41.5	0.33	0.24	0.64×10^6	44000
43	30	5.23×10^4	9.3	7.6	2.78×10^5	312	1.9	103	0.71	0.27	0.545×10^6	37000
46	35	6.30×10^4	9.5	9.0	2.11×10^5	201	2.2	183	1.07	0.32	1.07×10^6	59000
48	63	7.67×10^4	6.6	16	2.09×10^5	113	4.0	198	0.65	0.57	1.01×10^6	31000
51	54	4.85×10^4	4.8	14	1.81×10^5	97	3.4	80	0.31	0.49	0.84×10^6	33000
52	68	5.2×10^4	4.1	17	2.155×10^5	108	4.3	118	0.36	0.61	0.955×10^6	29000
53	68	3.3×10^4	2.6	17	1.62×10^5	81	4.3	135	0.41	0.61	0.81×10^6	25000
54	96	4.44×10^4	2.5	24	1.66×10^5	58	6.1	130	0.28	0.87	0.79×10^6	17000
57	86	3.83×10^4	2.4	22	1.83×10^5	72	5.4	156.5	0.38	0.78	0.92×10^6	21000
60	104	5.09 × 104	2.6	26	1.96×10^5	65	6.6	92	0.18	0.94	0.85×10^6	16500

[a] (dpm/m^2/d), from ocean ^{7}Be inventory.
[b] (nmol/m^2/d), from Eq. (1).
[c] Inventory, (nmol/m^2).
[d] Residence time (years), from Eqs. (1) and (7) and solubility in Table 5.
[e] Likely contamination.

assumed to be the true residence time. If additional input flux terms exist and are not accounted for, then this formulation will yield an apparent τ that is too high, particularly when compared to other remote surface ocean regions known to be dominated by atmospheric inputs. On the other hand, additional sinks (i.e. negative flux) would be manifest in an apparent τ that is too low. To account for additional flux terms,

$$\tau = M/(F_{TE(sol)} + F_x) \quad (9)$$

where F_x represents other dissolved TE sources (sinks), such that.

$$F_x = [M/\tau] - F_{TE(sol)} \quad (9b)$$

Application of Eq. (9b) implies that τ, the residence time with respect to atmospheric deposition, can be determined independently from stations where additional, non-atmospheric external sources or sinks are absent. The calculated apparent residence times are presented in Table 7 and illustrated in Fig. 6.

4.4.1. Fe

For most stations, Fe displayed a consistent residence time of 27 ± 11 y, which is only slightly longer than the 0.75–10 y range reported by Croot et al. (2004) for the eastern equatorial Atlantic but is much longer than those reported by others such as 0.6–0.8 y by Jickells (1999) for the Sargasso Sea, 0.5–1 y by Hayes et al. (2015) for the Central Pacific, and 6–14 months by Sarthou et al. (2007) for Atlantic waters influenced by the Saharan dust plume. These data suggest an inverse relationship of residence time to particle flux and might account for the longer apparent residence times reported here for the low-dust Arctic environment. Reductive porewater fluxes to Pacific waters over the Chukchi shelf might also constitute an additional iron input and lead to an apparently longer residence time (MacDonald and Gobeil, 2011). However, five stations (30–43) in the central Arctic display an apparent residence time of 465 ± 85 years, which is an unrealistically long timescale, even beyond the 70–300 y estimated for deep-ocean dissolved Fe (Bruland et al., 1994; Bergquist and Boyle, 2006). These stations are likely influenced by additional surface Fe input from the Transpolar Drift (TPD), which has been shown to convey shelf water properties to the central Arctic (e.g. Rutgers van der Loeff et al., 2012; Klunder et al., 2012; Kadko et al., 2016; Slagter et al., 2017; Rijkenberg et al., 2018; Kipp et al., 2018). The advective flux due to transport within the TPD can be estimated from Eq. (9b) under the assumption that the residence time of Fe in the TPD is similar to the residence time outside TPD influence. The mean atmospheric flux (derived from ^{7}Be) of soluble Fe for these stations, F_{TE}, was 0.61 ± 0.17 nmol/m^2/d, τ = 27y, (the average τ for stations not influenced by the TPD), and the mean dissolved Fe inventory (M) was ~ 100,000 nmol/m^2. Then, $F_x = F_{TPD}$ and is ~ 10 nmol/m^2/d for these stations, an order of magnitude greater than the soluble aerosol Fe atmospheric input.

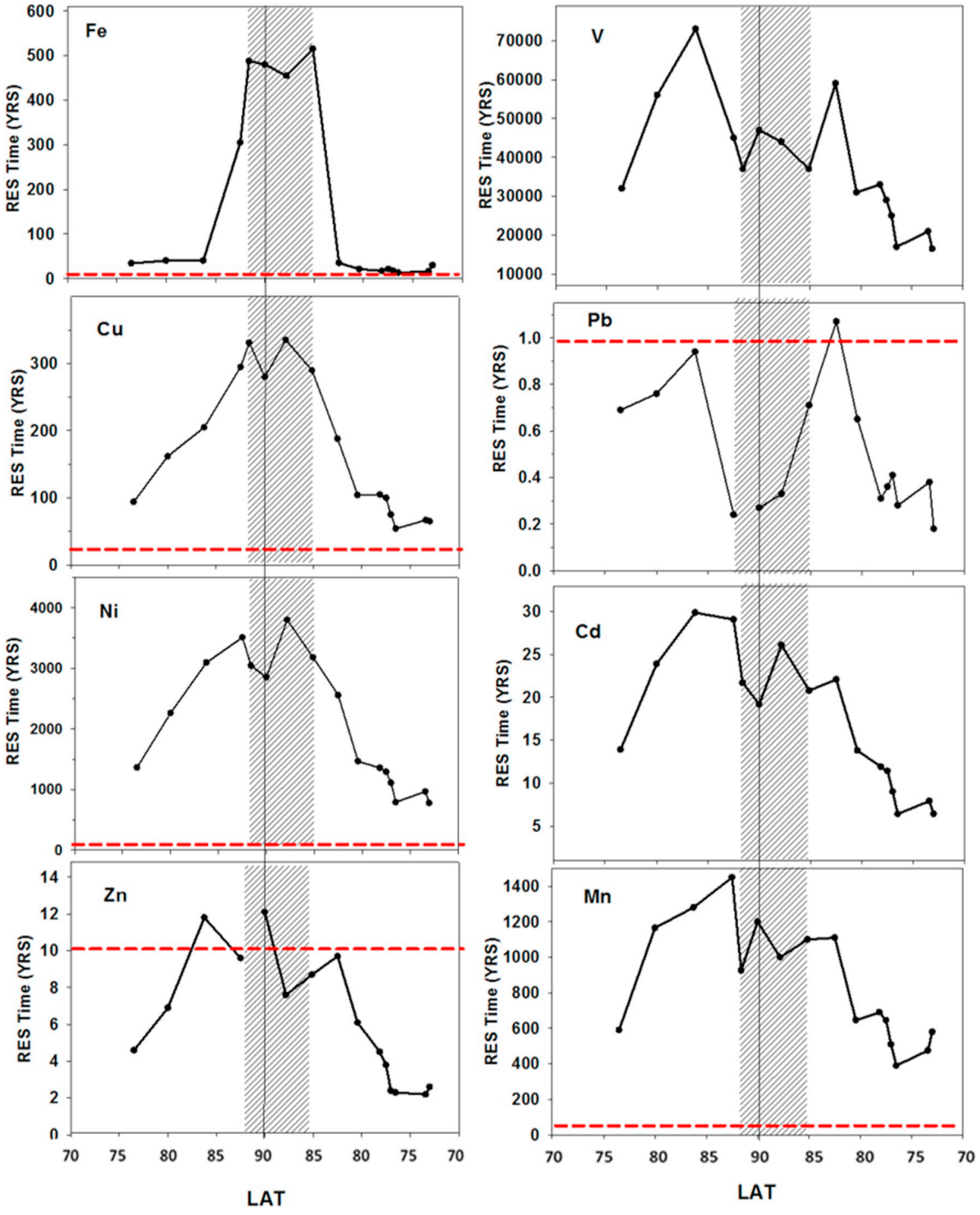

Fig. 6. Left column: Residence time plotted against latitude for elements showing enrichments in the TPD (Fe, Cu, Ni, Zn). Right column: Residence time plotted against latitude for elements showing a deficiency in the TPD (V,Pb) and for Mn and Cd which do not display an apparent relationship with the TPD. The shaded area represents the stations influenced by the TPD. The horizontal red dashed lines indicate residence times from prior literature in other ocean basins (see text). (For interpretation of the references to colour in this figure legend, the reader is referred to the web version of this article.)

4.4.2. Cu, Ni, Zn

The distributions of Cu, Ni and Zn also display influence from the TPD manifesting as increased residence times compared to non-TPD influenced stations (Fig. 6). Cu displayed an apparent residence time of 117 ± 56 years for non-TPD stations and 330 ± 28 years for TPD stations. For comparison, Bruland (1980) derived a dissolved Cu surface residence time with respect to atmospheric deposition of 10 years, and Boyle et al. (1977) 2.1–50 years with respect to scavenging, both for surface waters of the North Pacific. The approximate order of magnitude difference in apparent residence times between the Arctic and the North Pacific are likely due to additional Arctic riverine and/or shelf inputs. The mean atmospheric flux of soluble Cu for the TPD stations, F_{Cu}, was 1.90 ± 0.54 nmol/m^2/d, and the mean Cu inventory (M) was ~ 229,000 nmol/m^2. Thus, from Eq. (9b), F_{TPD} ~ 3.5 nmol/m^2/d which is twice the atmospheric flux at these stations.

Similarly, the apparent residence time of Ni in non-TPD stations was 1340 ± 690 years, which is nearly two orders of magnitude longer than the 20 years derived by Bruland (1980) in the North Pacific with

respect to atmospheric deposition. This again suggests that there must be additional sources of Ni beyond aerosols even to non-TPD stations, likely coming from rivers and/or shelf inputs. However, the apparent residence time for TPD stations is an even longer 2970 ± 430 years, indicating significant Ni inputs from the TPD. The mean apparent atmospheric flux of soluble Ni for the TPD stations was F_{Ni}, = 0.23 ± 0.07 nmol/m^2/d, and the mean Ni inventory (M) was ~ 284,000 nmol/m^2. Then F_{TPD} ~ 0.27 nmol/m^2/d, which is on the same order as the atmospheric flux.

For Zn, the residence time in non-TPD stations was 5.5 ± 3.1 years, which is within the range of 1 year reported by Bruland (1980) for the North Pacific, 12 ± 7 years reported by Sañudo-Wilhelmy et al. (2002) for surface waters near the Antarctic Peninsula, and 45 ± 23 years for the Atlantic sector of the Southern Ocean, reported by Croot et al. (2004). Thus, aerosol inputs may be the most significant source of Zn to the open Arctic, as for these other regions. For the TPD stations, the Zn residence time was 10.2 ± 2.0 years. The mean atmospheric flux of soluble Zn for the TPD stations was F_{Zn}, = 12.0 ± 3.4 nmol/m^2/d, and the mean inventory (M) was ~ 47,000 nmol/m^2. Then F_{TPD} was ~11.8 nmol/m^2/d which is on the order of the atmospheric flux.

4.4.3. V, Pb

The elements V and Pb show apparent residence times within TPD-influenced water that are lower than that of surrounding stations, suggesting removal of these elements from the source region of the TPD, likely the shelf areas of the east Siberian and Laptev Seas. Such processes might also be reflected in the lower residence times for these elements observed for stations 14, and 51–60, approaching the shallow Beaufort and Chukchi shelf regions as has been observed elsewhere (Shiller and Mao, 1999; Joung and Shiller, 2016). For V, the mean residence time for stations straddling the TPD stations (numbers 19, 26, 46, 48) is ~ 55,000 ± 17,000 years, dropping to 42,000 ± 4700 years within the TPD. The removal "sink" imprinted within the TPD can be estimated from Eq. (9b), where for V, the mean atmospheric flux of soluble V for the TPD stations F_{TE}, = 0.031 ± 0.009 nmol/m^2/d, τ = 55,000y, and the mean V inventory (M) is ~ 4.9 × 10^5 nmol/m^2. Then, $F_x = F_{TPD}$ and is ~ − 0.0066 nmol/m^2/d which is 21% of the atmospheric input.

For Pb, the residence time for stations straddling the TPD is 0.85 ± 0.19 y which is comparable to values in remote, aerosol flux-dominated regions such as 3 y in the North Pacific (Bruland, 1980) and < 1 y in the tropical N. Atlantic (Bridgestock et al., 2016). However the residence time drops to 0.39 ± 0.21 y for the TPD stations. Within the TPD stations the mean atmospheric flux of soluble Pb was F_{TE}, = 0.31 ± 0.09 nmol/m^2/d, and the mean Pb inventory (M) was ~ 50 nmol/m^2. Then, with τ = 0.85 y, F_{TPD} ~ − 0.15 nmol/m^2/d, which is 48% of the atmospheric input. This suggests that scavenging on the continental shelves may be a major sink of dissolved Pb from the Arctic Ocean.

4.4.4. Mn, Cd

The residence times with respect to atmospheric deposition of Mn and Cd show similar patterns across the GEOTRACES transect, whereby there is no obvious relationship to the TPD, but a suggestion of more rapid removal from surface waters at the marginal, shallow shelf areas. The mean apparent residence time of Cd is 17 ± 8 years, a timescale consistent with its measurement in corals as a tracer of historical natural and anthropogenic perturbations to the surface ocean (Shen et al., 1987). However, the apparent residence time of Mn (400–1400 y), is significantly greater than the ~20 years calculated for atmospheric input elsewhere (Jickells et al., 1994; Jickells, 1999; Shiller, 1997), suggesting appreciable input to the Arctic from other sources, most likely the Arctic shelves. Budget calculations suggest that about 90% of Mn input to the Arctic Ocean originates from Arctic rivers and coastal erosion/diagenetic fluxes from shelf sediments (MacDonald and Gobeil, 2011; Middag et al., 2011; Löwemark et al., 2014). Assuming τ = 20y, and with the observed inventory (M) of ~ ~200,000 nmol/m^2, Eq. (9b) yields a flux from these sources of ~30 nmol/m^2/d which is an order of magnitude greater than the atmospheric input of soluble Mn determined here (< 1 nmol/m^2/d).

5. Conclusions

There exist relatively few estimates of the residence time of atmospherically-delivered dissolved trace metals in the upper ocean, and heretofore none in the Arctic Ocean. This is mainly due to the difficulty in assessing atmospheric deposition rates and other source fluxes. In this work, the trace element flux into the upper Arctic Ocean was estimated by the ^{7}Be inventory and the TE/^{7}Be ratio of aerosols collected during the 2015 US Arctic GEOTRACES expedition. This method has been established elsewhere and was tested here by comparing the ^{7}Be-derived flux to the TE accumulation in recently deposited snow. Given the variability in snow and aerosol TE concentration observed over the limited observation period of the expedition, agreement between the two methods was reasonable. With knowledge of 1) the aerosol TE solubilities, and 2) the upper ocean inventory of dissolved TEs we calculated the mean apparent residence time of dissolved trace elements (TE) with respect to atmospheric deposition by assuming that atmospheric deposition was the dominant source flux at sites occupied across the GEOTRACES transect. This estimation was then compared to residence times determined for other remote regions dominated by atmospheric deposition to assess the importance of other input terms to the Arctic.

The apparent residence time with respect to atmospheric deposition for Fe was ~ 20–40 y for most stations. This is generally longer than those determined in other remote areas and might reflect weaker water column scavenging in the low-aerosol flux Arctic environment and/or additional sources of iron from reducing shelf sediments. Several stations that displayed an apparent residence time of ~300–500 years were likely influenced by additional input from the transpolar drift (TPD), which has been shown to convey shelf water properties to the central Arctic. This was seen for Cu, Ni and Zn as well. The flux of Fe delivered by the TPD was ~ 10 nmol/m^2/d for these stations, an order of magnitude greater than the soluble atmospheric input. The elements V and Pb showed apparent residence times within TPD-influenced water that are shorter than those at surrounding stations, suggesting removal of these elements from the source region of the TPD, likely the shelf areas of the east Siberian and Laptev Seas. The removal flux for Pb was 48% of its atmospheric input flux which suggests that scavenging on the continental shelves may be a major sink of dissolved Pb from the Arctic Ocean. For Mn, there was no obvious relationship of residence time with the TPD, however the apparent residence times (400–1400 yrs.) are significantly longer than the ~20 years calculated for atmospheric input elsewhere, suggesting appreciable input from other sources. Budget considerations have estimated that 90% of the dissolved Mn input to the Arctic Ocean originates from marginal areas of the Arctic Basin. Results here suggest a flux from these sources of ~30 nmol/m^2/d which is significantly greater than the atmospheric input of soluble Mn determined here (< 1 nmol/m^2/d).

Investigation of the processes that supply and remove trace elements in the ocean is an ongoing and active area of research, including understanding the source, residence time, and fate of atmospherically deposited trace elements into the ocean surface (e.g. Anderson et al., 2016; Baker et al., 2016). This is of particular importance for the Arctic, where decreasing ice cover and increased anthropogenic emissions suggest an evolving role of atmospheric deposition to the ocean chemistry and ecology of the region.

Acknowledgments

The authors thank the captain and crew of USCGC *Healy* for their

able field support. Mark Stephens, Kyle Dilliplaine, Greg Cutter, Gabrielle Weiss, Simone Moos, Pete Morton and Paul Aguilar provided important at-sea and laboratory technical assistance. Data have been submitted to The Biological and Chemical Oceanography Data Management Office (BCO-DMO). The authors thank Dr. M. Rutgers van der Loeff and two anonymous reviewers for their comments. This work was supported by the Chemical Oceanography Program of the NSF, grants OCE-1434085 (to DK), OCE- 1436312 (to AMS), OCE-1433717 (to AAI and RR), OCE- 1438047 (to CB), OCE- 1437266 (to WML), OCE-1434479 (to RA) and OCE 1434493 and 1713677 (to JNF).

Appendix A. Supplementary data

Supplementary data to this article can be found online at https://doi.org/10.1016/j.marchem.2018.10.011.

References

Aaboe, E., Dion, E.P., Turekian, K.K., 1981. 7Be in Sargasso sea and long Island sound waters. J. Geophys. Res. 86, 3255–3257.

Anderson, R.F., Cheng, H., Edwards, R.L., Fleisher, M.Q., Hayes, C.T., Huang, K.-F., Kadko, D., Lam, P.J., Landing, W.M., Lao, Y., Lu, Y., Measures, C.I., Morton, P.L., Moran, S.B., Ohnemus, D.C., Robinson, L.F., Shelley, R.U., 2016. How well can we quantify dust deposition to the ocean? Phil. Trans. R. Soc. A 374. https://doi.org/10.1098/rsta.2015.0285.

Arimoto, R., Snow, J.A., Graustein, W.C., Moody, J.L., Ray, B.J., Duce, R.A., Turekian, K.K., Maring, H.B., 1999. Influences of atmospheric transport pathways on radionuclide activities in aerosol particles from over the North Atlantic. J. Geophys. Res. 104 (D17), 21,301–21,316. https://doi.org/10.1029/1999JD900356.

Baker, A.R., Landing, W.M., Bucciarelli, E., Cheize, M., Fietz, S., Hayes, C.T., Kadko, D., Morton, P.L., Rogan, N., Sarthou, G., Shelley, R.U., Shi, Z., Shiller, A., van Hulten, M.M.P., 2016. Trace element and isotope exchange at the air – sea interface: progress and research needs. Phil. Trans. R. Soc. A. https://doi.org/10.1098/rsta.2016.0190.

Barrie, L.A., 1986. Arctic air pollution: a review of current knowledge. Atmos. Environ. 20, 643–663.

Bergquist, B.A., Boyle, E.A., 2006. Dissolved iron in the tropical and subtropical Atlantic Ocean, Global Biogeochem. Cycle 20, GB1015. https://doi.org/10.1029/2005GB002505.

Boyle, E.A., Sclater, F.R., Edmond, J.M., 1977. The distribution of dissolved copper in the Pacific. Earth Planet. Sci. Lett. 37, 38–54.

Bridgestock, L., van de Flierdt, T.V., Rehkamper, M., Paul, M., Middag, R., Milne, A., Lohan, M.C., Baker, A.R., Chance, R., Khondoker, R., Strekopytov, S., Humphreys-Williams, E., Achterberg, E.P., Rijkenberg, M.J.A., Gerringa, L.J.A., de Baar, H.J.W., 2016. Return of naturally sourced Pb to Atlantic surface waters. Nat. Commun. 7. https://doi.org/10.1038/ncomms12921.

Bruland, K., 1980. Oceanographic distributions of cadmium, zinc, nickel, and copper in the north Pacific. Earth Planet. Sci. Lett. 47, 176–198.

Bruland, K.W., Orians, K.J., Cowen, J.P., 1994. Reactive trace metals in the stratified central North Pacific. Geochim. Cosmochim. Acta 58, 3171–3182.

Buck, C.S., Landing, W.M., Resing, J.A., Lebon, G.T., 2006. Aerosol iron and aluminum solubility in the northwest Pacific Ocean: results from the 2002 IOC Cruise. Geochem. Geophys. Geosyst. 7, Q04M07. https://doi.org/10.1029/2005GC000977.

Cámara-Mor, P., Masque, P., Garcia-Orellana, J., Kern, S., Cochran, J.K., Hanfland, C., 2011. Interception of atmospheric fluxes by Arctic sea ice: evidence from cosmogenic 7Be. J. Geophy. Res. 116, C12041. https://doi.org/10.1029/2010JC006847.

Croot, P.L., Streu, P., Baker, A.R., 2004. Short residence time for iron in surface seawater impacted by atmospheric dry deposition from Saharan dust events. Geophys. Res. Lett. 31. https://doi.org/10.1029/2004GL020153.

Cutter, G.A., Bruland, K.W., 2012. Rapid and noncontaminating sampling system for trace elements in a global ocean surveys. Limnol. Oceanogr. Meth. 10, 425–436.

Davidson, C.I., Chu, L., Grimm, T.C., Nasta, M.A., Qamoos, M.P., 1981. Wet and dry deposition of trace element onto the Greenland ice sheet. Atmos. Environ. 15, 1429–1437.

Davidson, C.I., Santhanam, S., Fortmann, R.C., Olsen, M.P., 1985. Atmospheric transport and deposition of trace elements onto the Greenland ice sheet. Atmos. Environ. 19, 2065–2081.

Dibb, J.E., Meeker, D.L., Finkel, R.C., Southon, J.R., Caffee, M.W., Barrie, L., 1994. Estimation of stratospheric input to the Arctic troposphere: 7Be and 10Be in aerosols at Alert. Can. J. Geophy. Res. 99 (12), 855–12,864 D6.

Dimento, B.P., R.P. Mason, S. Brooks, C. Moore (submitted) the impact of sea ice on the air-sea exchange of mercury in the Arctic Ocean. Deep-Sea Res. I Oceanogr. Res. Pap.

Douglas, T.A., Sturm, M., 2004. Arctic haze, mercury and the chemical composition of snow across northwestern Alaska. Atmos. Environ. 38, 805–820.

Eicken, H., Krouse, H.R., Kadko, D., Perovich, D.K., 2002. Tracer studies of pathways and rates of meltwater transport through Arctic summer sea ice. J. Geophys. Res. 107 (C10), 8046. https://doi.org/10.1029/2000JC000583.

Feely, H.W, Larsen, R.J., Sanderson, C.G., 1989. Factors that cause seasonal variations in Beryllium-7 concentrations in surface air. J. Environ. Radioactiv. 9, 223–249. https://doi.org/10.1016/0265-931X(89)90046-5.

Fetterer, F., Untersteiner, N., 1998. Observations of melt ponds on arctic sea ice. J. Geophys. Res. 103, 24,821–24,835.

Frossard, A.A., Shaw, P.M., Russell, L.M., Kroll, J.H., Canagaratna, M.R., Worsnop, D.R., Quinn, P.K., Bates, T.S., 2011. Springtime Arctic haze contributions of submicron organic particles from European and Asian combustion sources. J. Geophys. Res. 116, D05205. https://doi.org/10.1029/2010JD015178.

Haskell, W.Z., Kadko, D., Hammond, D.E., Prokopenko, M.G., Berelson, W.M., Knapp, A.N., Capone, D., 2015. Upwelling velocities and eddy diffusivity from ^{7}Be measurements used to compare vertical nutrient fluxes to export POC flux in the Eastern Tropical South Pacific. Mar. Chem. 168, 140–150. https://doi.org/10.1016/j.marchem.2014.10.004.

Hathorne, E.C., Haley, B., Stichel, T., Grasse, P., Zieringer, M., Frank, M., 2012. Online preconcentration ICP-MS analysis of rare earth elements in seawater. Geochem. Geophys. Geosyst. 13, Q01020. https://doi.org/10.1029/2011GC003907.

Hayes, C.T., Fitzsimmons, J.N., Boyle, E.A., McGee, D., Anderson, R.F., Weisend, R., Morton, P.L., 2015. Thorium isotopes tracing the iron cycle at the Hawaii Ocean Time-series Station ALOHA. Geochim. Cosmochim. Acta 169, 1–16. https://doi.org/10.1016/j.gca.2015.07.019.

Hov, O., Shepson, P., Wolff, E., 2007. The chemical composition of the polar atmosphere—the IPY contribution. Bull. World Meteorol. Organ. 56, 263–269.

Jickells, T.D., 1999. The inputs of dust derived elements to the Sargasso Sea; a synthesis. Mar. Chem. 68, 5–14.

Jickells, T., Church, T., Veron, A., Arimoto, R., 1994. Atmospheric inputs of manganese and aluminum to the Sargasso Sea and their relation to surface water concentrations. Mar. Chem. 46, 283 292.

Joung, D., Shiller, A.M., 2016. Temporal and spatial variations of dissolved and colloidal trace elements in Louisiana Shelf waters. Mar. Chem. 181, 25–43.

Kadko, D., 2000. Modeling the evolution of the arctic mixed layer during the fall 1997 SHEBA project using measurements of 7Be. J. Geophys. Res 105, 3369–3378.

Kadko, D., Johns, W., 2011. Inferring upwelling rates in the equatorial Atlantic using 7Be measurements in the upper ocean. Deep-Sea Res. I. https://doi.org/10.1016/j.dsr.2011.03.004.

Kadko, D., Olson, D., 1996. Be-7 as a tracer of surface water subduction and mixed layer history. Deep-Sea Res. 43, 89–116.

Kadko, D., Prospero, J., 2011. Deposition of 7Be to Bermuda and the regional ocean: environmental factors affecting estimates of atmospheric flux to the ocean. J. Geophys. Res. 116, C02013. https://doi.org/10.1029/2010JC006629.

Kadko, D., Swart, P., 2004. The source of the high heat and freshwater content of the upper ocean at the SHEBA site in the Beaufort Sea in 1997. J. Geophys. Res. 109, C01022. https://doi.org/10.1029/2002JC001734.

Kadko, D., Landing, W.M., Shelley, R.U., 2015. A novel tracer technique to quantify the atmospheric flux of trace elements to remote ocean regions. J. Geophy. Res. Oceans 119. https://doi.org/10.1002/2014JC010314.

Kadko, D., Galfond, B., Landing, W.M., Shelley, R.U., 2016. Determining the pathways, fate, and flux of atmospherically derived trace elements in the arctic ocean/ice system. Mar. Chem. 182, 38–50. https://doi.org/10.1016/j.marchem.2016.04.006.

Kipp, L.E., Charette, M.A., Moore, W.S., Henderson, P.B., Rigor, I.G., 2018. Increased fluxes of shelf-derived materials to the Central Arctic Ocean. Sci. Adv. 4 (1). https://doi.org/10.1126/sciadv.aao1302.

Klunder, M.B., Bauch, D., Laan, P., de Baar, H.J.W., van Heuven, S., Ober, S., 2012. Dissolved iron in the Arctic shelf seas and surface waters of the central Arctic Ocean: impact of Arctic river water and ice-melt. J. Geophys. Res. 117, C01027. https://doi.org/10.1029/2011JC007133.

Krishnaswami, S., Lal, D., Somayajulu, B.L.K., Dixon, F.S., Stonecipher, S.A., Craig, H., 1972. Silicon, radium, thorium and lead in seawater: In-situ extraction by synthetic fibre. Earth Planet. Sci. Lett. 16, 84–90. https://doi.org/10.1016/0012-821X(72)90240-3.

Lagerström, M.E., Field, M.P., Séguret, M., Fischer, L., Hann, S., Sherrell, R.M., 2013. Automated on-line flow-injection ICP-MS determination of trace metals (Mn, Fe, Co, Ni, Cu and Zn) in open ocean seawater: Application to the GEOTRACES program. Mar. Chem. 155, 71–80. https://doi.org/10.1016/j.marchem.2013.06.001.

Lal, D., Chung, Y., Platt, T., Lee, T., 1988. Twin cosmogenic radiotracer studies of phosphorus recycling and chemical fluxes in the upper ocean. Limnol. Oceanogr. 336, 1559–1567.

Law, K., Stohl, A., 2007. Arctic Air Pollution: Origins and Impacts. Science 315, 1537–1540.

Lee, T., Barg, E., Lal, D., 1991. Studies of vertical mixing in the Southern California Bight with cosmogenic radionuclides radionuclides 32P and 7Be. Limnol. Oceanogr. 365, 1044–1053.

Löwemark, L., Marz, C., O'Regan, M., Gyllencreutz, R., 2014. Arctic Ocean Mn-stratigraphy : genesis, synthesis and inter-basin correlation. Quat. Sci. Rev. 92.

MacDonald, R.W., Gobeil, C., 2011. Manganese sources and sinks in the arctic ocean with reference to periodic enrichments in basin sediments. Aquat. Geochem. 18, 565–591. https://doi.org/10.1007/s10498-011-9149-9.

Marsay, C.M., Kadko, D., Landing, W.M., Morton, P.L., Summers, B.A., Buck, C.S., 2018a. Concentrations, provenance and flux of aerosol trace elements during US GEOTRACES Western Arctic cruise GN01. Chem. Geol. https://doi.org/10.1016/j.chemgeo.2018.06.007.

Marsay, C.M., Aguilar-Islas, A., Fitzsimmons, J.N., Hatta, M., Jensen, L.T., John, S.G., Kadko, D., Landing, W., Lanning, N.T., Morton, P.L., Pasqualini, A., Rauschenberg, S., Sherrell, R.M., Shiller, A.M., Twining, B.S., Whitmore, L.M., Zhange, R., Buck, C.S., 2018b. Dissolved and particulate trace elements in late summer Arctic melt ponds. Mar. Chem. doi. https://doi.org/10.1016/j.marchem.2018.06.002.

Maykut, G.A., McPhee, M.G., 1995. Solar heating of the Arctic mixed layer. J. Geophys. Res. 100 (24), 691–24, 703.

Middag, R., de Baar, H.J.W., Laan, P., Klunder, M.B., 2011. Fluvial and hydrothermal input of manganese into the Arctic Ocean. Geochim. Cos. Acta. 75, 2393–2408.

Morison, J.H., Smith, J.D., 1981. Seasonal variations in the upper Arctic as observed at T-3. Geophys. Res. Lett. 8, 753–756.
Ohnemus, D.C., Sherrell, R.M., Lagerstöm, M., Morton, P.L., Twining, B.S., Rauschenberg, S.M., Auro, M.E., Lam, P.J., 2014. Piranha a chemical method for dissolution of polyethersulfone filters and laboratory inter-comparison of marine particulate digests. Limnol. Oceanogr. Methods 12, 530–547. https://doi.org/10.4319/lom.2014.12.530.
Olsen, C.R., Larsen, I.L., Lowry, P.D., Cutshell, N.H., 1986. Geochemistry and deposition of 7Be in riverine and coastal waters. J. Geophys. Res. 91, 896–908.
Pacyna, J.M., Ottar, B., 1985. Transport and chemical composition of the summer aerosol in the Norwegian Arctic. Atmos. Env. 19 (12), 2109–2120.
Rijkenberg, M.J.A., Slagter, H.A., Rutgers Van Der Loeff, M., van Ooijen, J., Gerringa, L.J.A., 2018. Dissolved Fe in the deep and Upper Arctic Ocean with a focus on Fe limitation in the Nansen Basin. Front. Mar. Sci. 5, 88. https://doi.org/10.3389/fmars.2018.00088.
Rutgers van der Loeff, M., Cai, P., Stimac, I., Bauch, D., Hanfland, C., Roeske, T., Moran, S.B., 2012. Shelf-basin exchange times of Arctic surface waters estimated from 228Th/228Ra disequilibrium. J. Geophys. Res. 117, C03024. https://doi.org/10.1029/2011JC007478.
Sañudo-Wilhelmy, S.A., Olsen, K.A., Scelfo, J.M., Foster, T.D., Flegal, A.R., 2002. Trace metal distributions off the Antarctic Peninsula in the Weddell Sea. Mar. Chem. 77, 157–170.
Sarthou, G.A.R., Baker, J., Kramer, P., Laan, A., Laësa, S., Ussher, E.P., Achterberge, H.J.W., de Baar, K.R., Timmermans, S. Blain, 2007. Influence of atmospheric inputs on the iron distribution in the Subtropical North-East Atlantic Ocean. Mar. Chem. https://doi.org/10.1016/j.marchem.2006.11.004.
Shaw, G.E., 1995. The arctic haze phenomenon. Bull. Am. Meteorol. Soc. 76, 2403–2413.
Shelley, R.U., Roca-Marti, M., Castrillejo, M., Masque, P., Landing, W.M., Planquette, H., Sarthou, G., 2017. Quantification of trace element atmospheric deposition fluxes to the Atlantic Ocean (> 40°N; GEOVIDE, GEOTRACES GA01) during spring 2014. Deep-Sea Res. I. 119, 34–49.
Shen, G.T., Boyle, E.A., Lea, D.W., 1987. Cadmium in corals as a tracer of historical upwelling and industrial fallout. Nature 328, 794–796.
Shiller, A.M., 1997. Manganese in surface waters of the Atlantic Ocean. Geophysical Res. Lett. 24, 1495–1498.
Shiller, A.M., Mao, L., 1999. Dissolved vanadium on the Louisiana Shelf: effect of oxygen depletion. Cont. Shelf Res. 19, 1007–1020.
Sirois, A., Barrie, L.A., 1999. Arctic lower tropospheric aerosol trends and composition at Alert, Canada: 1980–1995. JGR 104 (D9), 11599–11618.
Skyllingstad, E.D., Paulson, C.A., 2007. A numerical study of melt ponds. J. Geophys. Res. 112, C08015. https://doi.org/10.1029/2006JC003729.
Slagter, H.A., Reader, H.E., Rijkenberg, M.J.A., Rutgers Van Der Loeff, M., de Baar, H.J.W., Gerringa, L.J.A., 2017. Organic Fe speciation in the Eurasian basins of the Arctic Ocean and its relation to terrestrial DOM. Mar. Chem. 197, 11–25 (doi: 0.1016/j.marchem. 2017.10.005).
Stohl, A., 2006. Characteristics of atmospheric transport into the Arctic troposphere. J. Geophy. Res. 111, D11306. https://doi.org/10.1029/2005JD006888.
Tschudi, M.A., Maslanik, J.A., Perovich, D.K., 2008. Derivation of melt pond coverage on Arctic sea ice using MODIS observations. Remote Sens. Environ. 112, 2014–2605.
Turekian, K.K., Benninger, L.K., Dion, E.P., 1983. 7Be and 210Pb total depositional fluxes at New Haven, Connecticut and Bermuda. J. Geophys. Res. 88, 5411–5415.
Warren, S.G., Rigor, I.G., Untersteiner, N., Radionov, V.F., Bryazgin, N.N., Aleksandrov, Ye.I., Colony, R., 1999. Snow depth on Arctic sea ice. J. Climate 12, 1814–1829.
Young, J.A., Silker, W.B., 1980. Aerosol deposition velocities on the Pacific and Atlanic Oceans calculated from 7Be measurements. Earth Planet. Sci. Lett. 50, 92–104. https://doi.org/10.1016/ 0012-821X(80)90121-1.
Zhan, J., Gao, Y., 2014. Impact of summertime anthropogenic emissions on atmospheric black carbon at Ny-Ålesund in the Arctic. Polar Res. 33, 1. https://doi.org/10.3402/polar.v33.21821.